Monthly Notices
of the
ROYAL ASTRONOMICAL SOCIETY

MNRAS **494,** 5230–5238 (2020)
Advance Access publication 2020 April 22

doi:10.1093/mnras/staa1085

Enhanced mass-loss rate evolution of stars with $\gtrsim$18 $M_\odot$ and missing optically observed type II core-collapse supernovae

Roni Anna Gofman,[1]★ Naomi Gluck[2] and Noam Soker[1,3]

[1]*Department of Physics, Technion, Haifa 3200003, Israel*
[2]*Department of Physics, Stony Brook University, Stony Brook, New York 11794-3800, USA*
[3]*Guangdong Technion Israel Institute of Technology, Shantou 515069, Guangdong Province, China*

Accepted 2020 April 16. Received 2020 April 8; in original form 2019 October 24

ABSTRACT

We evolve stellar models with zero-age main-sequence (ZAMS) mass of $M_{\rm ZAMS} \gtrsim 18\,{\rm M}_\odot$ under the assumption that they experience an enhanced mass-loss rate when crossing the instability strip at high luminosities and conclude that most of them end as type Ibc supernovae (SNe Ibc) or dust-obscured SNe II. We explore what level of enhanced mass-loss rate during the instability strip would be necessary to explain the 'red supergiant problem'. This problem refers to the dearth of observed core-collapse supernovae progenitors with $M_{\rm ZAMS} \gtrsim 18\,{\rm M}_\odot$. Namely, we examine what enhanced mass-loss rate could make it possible for all these stars actually to explode as core-collapse supernovae (CCSNe). We find that the mass-loss rate should increase by a factor of at least about 10. We reach this conclusion by analysing the hydrogen mass in the stellar envelope and the optical depth of the dusty wind at the explosion, and crudely estimate that under our assumptions only about a fifth of these stars explode as unobscured SNe II and SNe IIb. About 10–15 per cent end as obscured SNe II that are infrared-bright but visibly very faint, and the rest, about 65–70 per cent, end as SNe Ibc. However, the statistical uncertainties are still too significant to decide whether many stars with $M_{\rm ZAMS} \gtrsim 18\,{\rm M}_\odot$ do not explode as expected in the neutrino driven explosion mechanism, or whether all of them explode as CCSNe, as expected by the jittering jets explosion mechanism.

Key words: stars: massive – stars: mass-loss – supernovae: general – stars: winds, outflows.

1 INTRODUCTION

The two theoretical mechanisms to power core-collapse supernova (CCSN) explosions from the gravitational energy that the collapsing core releases are: the delayed neutrino mechanism (Bethe & Wilson 1985), and the jittering jets explosion mechanism (Soker 2010; or more generally the jet feedback mechanism, e.g. Soker 2016). Each of these mechanisms in its originally proposed form encounters some problems that require the addition of some ingredients.

The extra ingredient that recent numerical simulations of the delayed neutrino mechanism introduce to overcome some of the basic problems of the original delayed neutrino mechanism (for these problems, see e.g. Kushnir 2015; Papish, Nordhaus & Soker 2015) is convection above the iron core in the pre-collapse core (e.g. Couch & Ott 2013, 2015; Mueller & Janka 2015; Müller et al. 2017, 2019). The flow fluctuations of the convective zone that ease explosion results in large-amplitude stochastic angular momentum variations of the mass that the newly born neutron star (NS) accretes. These fluctuations seem to lead to the launching of a bipolar outflow with varying symmetry axis directions, namely, jittering jets (Soker 2019b).

Indeed, the jittering jets explosion mechanism is based on such flow fluctuations in the convective regions of the pre-collapse core or envelope (Gilkis & Soker 2014, 2015; Quataert, Lecoanet & Coughlin 2019). The spiral standing accretion shock instability (SASI) and other instabilities behind the stalled shock at about 100 km from the newly born NS amplify these fluctuations (for the physics of the spiral SASI, see e.g. Blondin & Mezzacappa 2007; Iwakami, Nagakura & Yamada 2014; Kuroda, Takiwaki & Kotake 2014; Fernández 2015; Kazeroni, Guilet & Foglizzo 2017). However, results of numerical simulations that find no stochastic accretion discs around the newly born NS brought to the recognition that neutrino heating plays a role in the jittering jets explosion mechanism (Soker 2018, 2019a). In a recent study, Soker (2019b) analyses three-dimensional hydrodynamical simulations of CCSNe and concludes that both neutrino heating and accretion of stochastic angular momentum operate together to launch jittering jets that explode CCSNe.

One of the places where the delayed neutrino mechanism and the jittering jets explosion mechanism differ from each other is the prediction of the outcome of stars with zero-age main-sequence

★ E-mail: rongof@campus.technion.ac.il

(ZAMS) mass of $M_{\rm ZAMS} \gtrsim 18\,{\rm M}_\odot$. According to the delayed neutrino mechanism for most of the masses in that range the core-collapses to form a black hole in a failed supernova, i.e. there is no explosion (e.g. Fryer 1999; Horiuchi et al. 2014; Ertl et al. 2016; Sukhbold et al. 2016; Ertl et al. 2019; Sukhbold & Adams 2019), but rather only a faint transient event (Nadezhin 1980; Lovegrove & Woosley 2013). According to the jittering jets explosion mechanism, on the contrary, there are no failed CCSNe, and all of these stars do explode, even if the collapsing core forms a black hole. According to the jittering jets explosion mechanism when a black hole is formed the outer core material and then the envelope gas contains enough stochastic angular momentum (e.g. Gilkis & Soker 2014, 2015; Quataert et al. 2019) to launch jets and set an energetic explosion, up to $E_{\rm exp} > 10^{52}$ erg (Gilkis, Soker & Papish 2016).

These different predictions of the two explosion mechanisms relate directly to the so-called 'red supergiant (RSG) problem' (Smartt et al. 2009), referring to the finding that the observed relative number of progenitors of CCSNe II with ZAMS masses of $M_{\rm ZAMS} \gtrsim 18\,{\rm M}_\odot$ is much lower than their relative number on the main sequence (e.g. Jennings et al. 2014; Williams et al. 2014; for a review, see e.g. Smartt 2015). Smartt (2015) argues in his thorough review of the 'red supergiant problem' that it is consistent with the claim of the delayed neutrino mechanism that most stars of $M_{\rm ZAMS} \gtrsim 18\,{\rm M}_\odot$ collapse to form black holes with no visible supernovae, but possibly a faint transient event. Adams et al. (2017) suggest that the star N6946-BH1 that erupted in 2009 (Gerke, Kochanek & Stanek 2015) was a failed SN event of a progenitor of $\approx 25\,{\rm M}_\odot$. Kashi & Soker (2017) provide an alternative interpretation to that event based on a transient event (intermediate luminosity optical transient – ILOT) that was obscured by dust in the equatorial plane that happens to be along our line of sight.

We do note that there are claims for massive progenitors of some CCSNe, e.g. a progenitor of the type IIn SN 2010jl of mass $M_{\rm ZAMS} \gtrsim 30\,{\rm M}_\odot$ (Smith et al. 2011), and a possible SN Ic progenitor with a mass of $M_{\rm ZAMS} \gtrsim 50\,{\rm M}_\odot$ (Van Dyk et al. 2018).

One possible explanation to the missing massive progenitors of CCSNe II might be an obscuration by dust (e.g. Walmswell & Eldridge 2012), but one should properly calculate dust extinction in CCSNe (Kochanek, Khan & Dai 2012).

Jencson et al. (2017) claim that if the two events they studied in the infrared (IR) are CCSNe, then-current optical surveys miss $\gtrsim$ 18 per cent of nearby CCSNe. In a more systematic study, Jencson et al. (2019) find nine IR bright transients, and estimate that five of these events are dust-obscured CCSNe (probably obscured by dusty clouds in the host galaxy). They further estimate that optical surveys miss $\approx$ 40 per cent (the range of 17–64 per cent) of all CCSNe. If holds, this might cover most (or even all) stars with $M_{\rm ZAMS} \gtrsim 18\,{\rm M}_\odot$, implying that these stars also explode as CCSNe.

The obscured CCSNe that Jencson et al. (2019) study are most likely obscured by dusty clouds in the host galaxy, rather by a dust circumstellar matter (CSM). We here raise the following question. What enhanced mass-loss rate during the RSG could make the CSM of some RSG with $M_{\rm ZAMS} \gtrsim 18\,{\rm M}_\odot$ sufficiently dense to obscure their explosion? We also add the related question of whether our assumed enhanced mass-loss rate might bring some RSG to explode as SNe Ibc rather than SNe II or IIb, even if they are not obscured by their own CSM.

Yoon & Cantiello (2010) already studied the process by which partial ionization of hydrogen in the envelope causes RSG stars to strongly pulsate and lose mass at a very high rate (e.g. Heger et al. 1997). They further discussed the possibility that this enhanced mass-loss rate of stars with $M_{\rm ZAMS} \gtrsim 19{-}20\,{\rm M}_\odot$ might explain the RSG problem, by both forming an optically thick dusty CSM and by removing most, or even all, of the hydrogen-rich envelope and forming a SN of type Ib or Ic (Ibc) progenitor. We continue the idea of Yoon & Cantiello (2010) but perform somewhat different evolutionary simulations. We assume that the stars have the enhanced mass-loss rate that we require to explain the RSG problem, when they cross the continuation of the instability strip on the HR diagram when they are RSGs. We strengthen the claim of Yoon & Cantiello (2010) that such an enhanced mass-loss rate might account for RSG problem, allowing all stars to explode as CCSNe. There are other studies that include enhanced mass-loss rate of stars during the RSG phase, but they do not compare directly to the RSG problem (e.g. Meynet et al. 2015).

In Section 2, we describe our numerical set-up, and in Section 3 we present the calculation of evolutionary tracks under the assumption that RSG stars that cross the instability strip have very high mass-loss rates. In Section 4, we study the enhanced mass-loss rate that would be necessary to obscure stars with $18\,{\rm M}_\odot \lesssim M_{\rm ZAMS} \lesssim 20\,{\rm M}_\odot$, and determine the role of this enhanced mass-loss rate in bringing more stars of $M_{\rm ZAMS} \gtrsim 20\,{\rm M}_\odot$ to explode as types IIb or Ib CCSNe. We summarize our main conclusions in Section 5.

2 NUMERICAL SET-UP

2.1 Stellar evolution

We evolve stellar models with ZAMS mass in the range of $M_{\rm ZAMS} = 15{-}30\,{\rm M}_\odot$ using Modules for Experiments in Stellar Astrophysics (MESA, version 10398; Paxton et al. 2011, 2013, 2015, 2018). Each model has an initial metallicity of $Z = 0.02$, and evolves from the pre-main-sequence stage until pre-core-collapse, which we take to be the first time the iron core has an inward velocity $\geq$ 1000 km.

We employ mixing according to a mixing-length theory (Henyey, Vardya & Bodenheimer 1965) with $\alpha_{\rm MLT} = 1.5$ in convective regions defined by the Ledoux criterion. Semiconvection is used with $\alpha_{\rm sc} = 1.0$ (Langer, Fricke & Sugimoto 1983). Step function convective overshooting is applied with an overshooting parameter of 0.335 (Brott et al. 2011).

We apply wind mass-loss with the MESA 'Dutch' mass-loss scheme for massive stars which combines results from several papers and is based on Glebbeek et al. (2009). For $T_{\rm eff} > 10^4$ K and surface hydrogen abundance larger than 0.4 the 'Dutch' scheme uses Vink, de Koter & Lamers (2001), and for surface hydrogen abundance lower than 0.4 it uses Nugis & Lamers (2000). In cases where $T_{\rm eff} < 10^4$ K, mass-loss is treated according to de Jager, Nieuwenhuijzen & van der Hucht (1988).

We break up the evolution to two parts: inside the instability strip and outside it. Fig. 1 in Georgy et al. (2013) shows the Hertzsprung–Russell (HR) diagram for non-rotating models with an instability strip in the range of $2 \lesssim \log(L/{\rm L}_\odot) \lesssim 5$ and $3.5 \lesssim \log(T_{\rm eff}\ [{\rm K}]) \lesssim 3.8$. From that figure, we approximate that the instability strip to be in the region where

$$64 \lesssim \log\left(\frac{L}{{\rm L}_\odot}\right) + 16.4 \log\left(\frac{T_{\rm eff}}{[{\rm K}]}\right) \lesssim 65. \quad (1)$$

We extend the instability strip from Georgy et al. (2013) to higher luminosities, by a linear continuation of the two boundaries of the strip on the HR diagram. Later we show that for the stars we evolve here, the centre of the instability strip continuation is at about an effective temperature of $\log(T_{\rm eff}) \simeq 3.6$. This is about the

same location on the HR diagram of the pulsating stars that Yoon & Cantiello (2010) study. As Yoon & Cantiello (2010) discuss, the pulsations are driven by partial ionization of hydrogen in the envelope. We further note that Yoon & Cantiello (2010) assume that these stars have pulsational-driven enhanced mass-loss rate. Although they did not show it from first principles, we accept here their assumption, but consider both moderate and large mass-loss rate enhancement (see Section 2.2).

While the star is outside the strip, we set the mass-loss scaling factor to $f_{\rm ml} = 0.8$ since the models have no rotation (Maeder & Meynet 2001). When the star crosses the extended part of the instability strip from right to left on the HR diagram, namely at very late evolutionary phases, we consider one of three cases for the mass-loss rate. In the first case, we assume that the instability strip has no special role, and we keep $f_{\rm ml} = 0.8$. The other two cases have enhanced mass-loss inside the instability strip. Once the model enters the strip from right to left we increase the mass-loss scaling factor to $f_{\rm ml} = 2$ in one case and to $f_{\rm ml} = 10$ in another.

As MESA is a numerical simulation code based on a grid (shells) and time-steps, we should show that there is a convergence, i.e. no dependence on the grid resolution for the value we use (e.g. Farmer et al. 2016). In MESA, there is a parameter 'maxdq' that sets the maximum mass in a shell, expressed as a fraction of total mass in the grid. We compared the default value of maxdq = 0.01 that we use in all our cases, to several cases that we simulated with higher resolution of maxdq = 10^{-3}. We found no differences in the pre-collapse characteristics we study in this paper.

The time-step control parameter 'deltalgXHcntrmin' sets the time-step as hydrogen is consumed in the core. Setting small time-step assists in calculating the passage from the ZAMS to the terminal-age main sequence. Similar parameters control the time-step for every significant evolution stage. We reduce the time-steps at these phases by setting these parameters to be 10^{-6} for hydrogen and helium (as in, e.g. Farmer et al. 2016), and 10^{-5} for heavier elements.

2.2 Enhanced mass-loss rate

Our question in this study is as follows. *By what factor should we increase the mass-loss rate during the RSG phase to explain the RSG problem?* We examine here two mass-loss rate enhancement factors (Section 2.1). We further assume, as we discussed above, that the enhanced mass-loss rate occurs only when the star crosses the instability strip from right to left, i.e. when it is very bright.

We emphasize that there is no observational justifications for this enhanced mass-loss rate (e.g. Beasor et al. 2020). As we mention in Section 1, based on their observations of dust-enshrouded CCSNe, Jencson et al. (2019) estimate that $\approx$ 17–64 per cent of all CCSNe are dust-enshrouded. In most (or even all) cases the obscuring dust is of ISM origin. Even if in some cases CSM obscures the CCSN, it might be that in the enhanced mass-loss rate of the progenitor was due to binary interaction.

We rather raise here a theoretical question: What should the enhanced mass-loss rate of single RSG stars be for single stars to explain the RSG problem? We find below (Sections 3 and 4) that to form a significant number of enshrouded CCSNe we need to increase the mass-loss rate of single stars in the instability strip by a factor of about 10 or somewhat larger (namely, $f_{\rm ml} \simeq 10$). Much lower values will not obscure the stars when explode, and much higher values will remove too much mass before explosion. Namely, we have no theoretical justification for taking $f_{\rm ml} \simeq 10$, but we rather claim that *if single stars form some dust-enshrouded CCSNe,* then the enhancement factor should be about 10 (here we take an enhancement factor of 12.5).

From the theoretical side, we base our prescription for enhanced mass-loss rate in the instability strip on the results of Yoon & Cantiello (2010) who argue that RSG stars lose mass at a very high rate when they are inside the instability strip on the HR diagram. There can be two basic regimes of the mass-loss rate enhancement because of pulsations in the instability strip. In the first the effect of the pulsations is linear, like the decrease in gravity and temperature as the envelope expands to maximum radius in the pulsation cycle. In this case the mass-loss rate increases by a moderate factor, which we here take to be 2.5 (for $f_{\rm ml} = 2$). In the other regime the effect is non-linear. For example, the lower temperature together with pulsation-driven shocks in the envelope lead to substantial extra dust formation (e.g. Goldman et al. 2017), with a large impact on the mass-loss rate. Here we take the increase of the mass-loss rate in the non-linear regime to be by a factor of 12.5 (for $f_{\rm ml} = 10$). As we discuss below, already in the linear regime we find a non-negligible influence of the enhanced mass-loss rate, that becomes quite significant in the non-linear regime.

The above discussion shows that from theoretical considerations the factor of $f_{\rm ml} = 10$ is arbitrary, as we have no derivation of the mass-loss rate increase due to the instability. However, as we explain above, we need the factor of $f_{\rm ml} \simeq 10$ to make sure that there is a significant number of dust-enshrouded CCSNe from single-star evolution.

We note that Meynet et al. (2015) conduct RSG evolution simulations where they increase the mass-loss rates by a factor of 10 and 25 relative to the standard mass-loss rates during the RSG phase. We return to the study of Meynet et al. (2015) in Section 3. Georgy (2012) also enhances the RSG mass-loss rate, by a factor of 3 and 10, but for lower masses than what we study, i.e. 12−15 $M_\odot$. Therefore, our enhanced mass-loss rate factor of up to 12.5 is not an extreme in such studies.

Finally, we note the following new results by Beasor et al. (2020). Beasor et al. (2020) study the mass-loss rate of RSGs in two stellar clusters, and conclude that the mass-loss rates they find are up to a factor of 20 lower than what current evolutionary models use. If the results of Beasor et al. (2020) hold by future studies, it would imply that to reach the desired mass-loss rate that leads to dust-enshrouded CCSNe we would have to increase the mass-loss rate relative to the value that Beasor et al. (2020) infer by a factor of $\approx$100 rather than by a factor of $\simeq$ 10. Namely, during most of the evolution the mass-loss rate is low, as suggested by Beasor et al. (2020), but some progenitors of CCSNe suffers very high mass-loss rate just before explosion due to enhanced mass-loss rate, or from binary interaction. Specifically, we find below that for single star to explain the RSG problem, in cases of obscured CCSNe the average mass-loss rate hundreds of years before explosion should be $\dot{M} \gtrsim 3 \times 10^{-5}\,M_\odot\,{\rm yr}^{-1}$. There is a clear need for further observations and theoretical study to explore the full behaviour of mass-loss from RSG.

3 RESULTS

In this section, we focus mostly on the effect of the mass-loss rate inside the instability strip on the pre-collapse state of the stellar models. We evolve over 40 stellar models up to the point of core-collapse with 16 different values of ZAMS mass for each of the three mass-loss parameters, $f_{\rm ml}$, that we set in the instability strip.

Fig. 1 shows the evolution of some models on the HR diagram, while for others we show only the final position. We also present

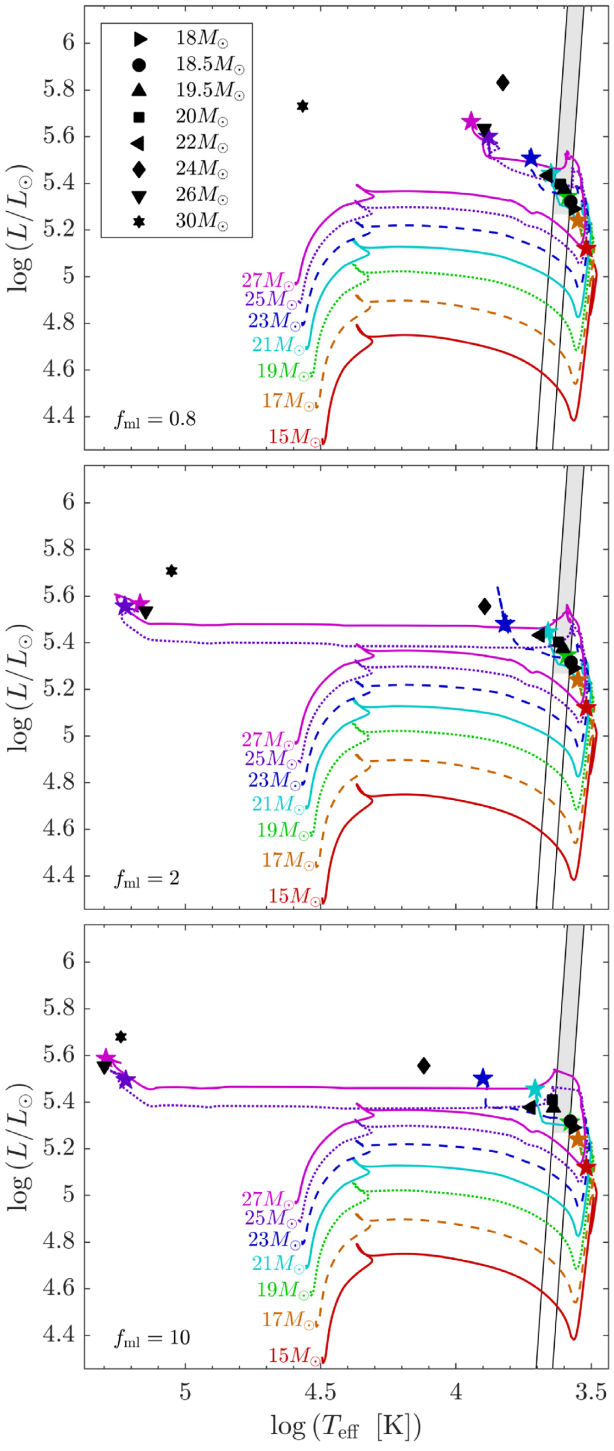

Figure 1. The evolution track of stellar models with ZAMS masses in the range of 15−30 $M_\odot$ from ZAMS to core-collapse on the HR diagram. The pre-collapse point of each model is marked by a coloured pentagram for odd masses and a black marker for all other masses. The instability strip and its extension according to equation (1) is marked with two black lines. The panels have different mass-loss scaling factors, $f_{\rm ml}$ as given in the inset when a star crosses the instability strip from right to left in the grey area of the strip.

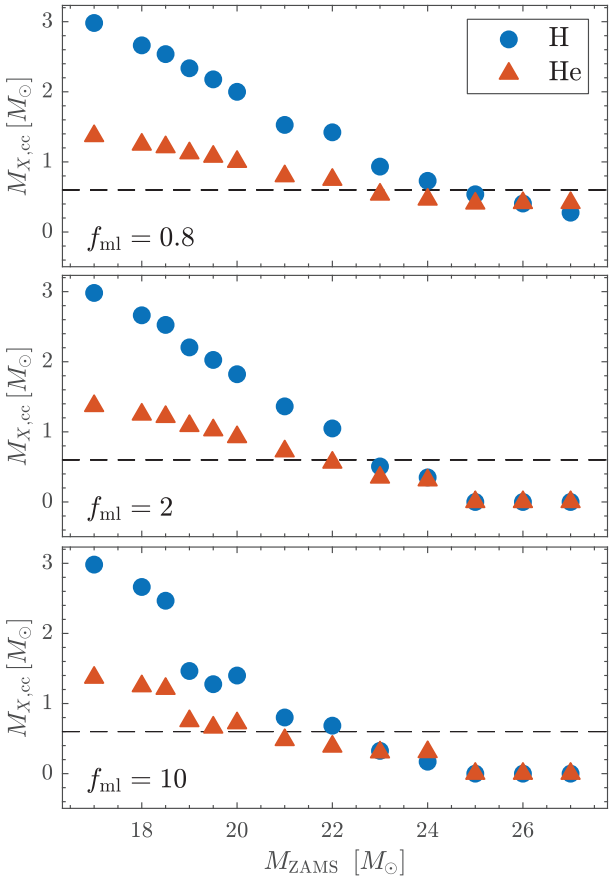

Figure 2. The final envelope mass of hydrogen (blue circles) and helium (orange triangles) as a function of the ZAMS mass. The three panels are for different mass-loss rate scaling factor, $f_{\rm ml}$, inside the instability strip as the star crosses from right to left in the HR diagram. Although the helium mass in the envelope of the most massive three models in the lower two panels is zero, there is a helium mass of about 2 $M_\odot$ in the core. Therefore, these will explode as SNe Ib.

the instability strip, including our extension to high luminosity. It is evident that by increasing the mass-loss rate when the star is inside the instability strip (extension) and crosses from right to left, the pre-collapse effective temperature of models that leave the strip increases.

Moreover, models with $M_{\rm ZAMS} \gtrsim 24$ $M_\odot$ and enhanced mass-loss rate in the instability strip lose their entire hydrogen envelope, as we show for in Fig. 2, and become hot progenitors of SNe Ib, i.e. Wolf–Rayet (WR) stars. Fig. 2 shows that stars with $M_{\rm ZAMS} \gtrsim 24\,M_\odot$ and enhanced mass-loss rate do not have hydrogen and helium in their envelope at explosion; this is because these stars loses there entire envelope by that time. These stars will explode as SNe Ib because they have a core helium layer of $\approx$2 $M_\odot$. Other models lose most of their hydrogen envelope but still are left with $0.01\,M_\odot \lesssim M_{\rm H,cc} \lesssim 0.5$–$1\,M_\odot$ of hydrogen in there envelope at core-collapse; these become the progenitors of SNe IIb. We explain the different groups and their implications on the RSG problem with more detail in Section 4.

Now we turn to examine the possibility of obscured CCSNe. We assume that the dense wind efficiently forms dust and calculate its optical depth. We consider the wind section from an inner radius of $R_{\rm in} = 0.5$–2×10^{16} cm, as we take the supernova to destroy dust at inner radii (calculating the exact radius requires to follow the

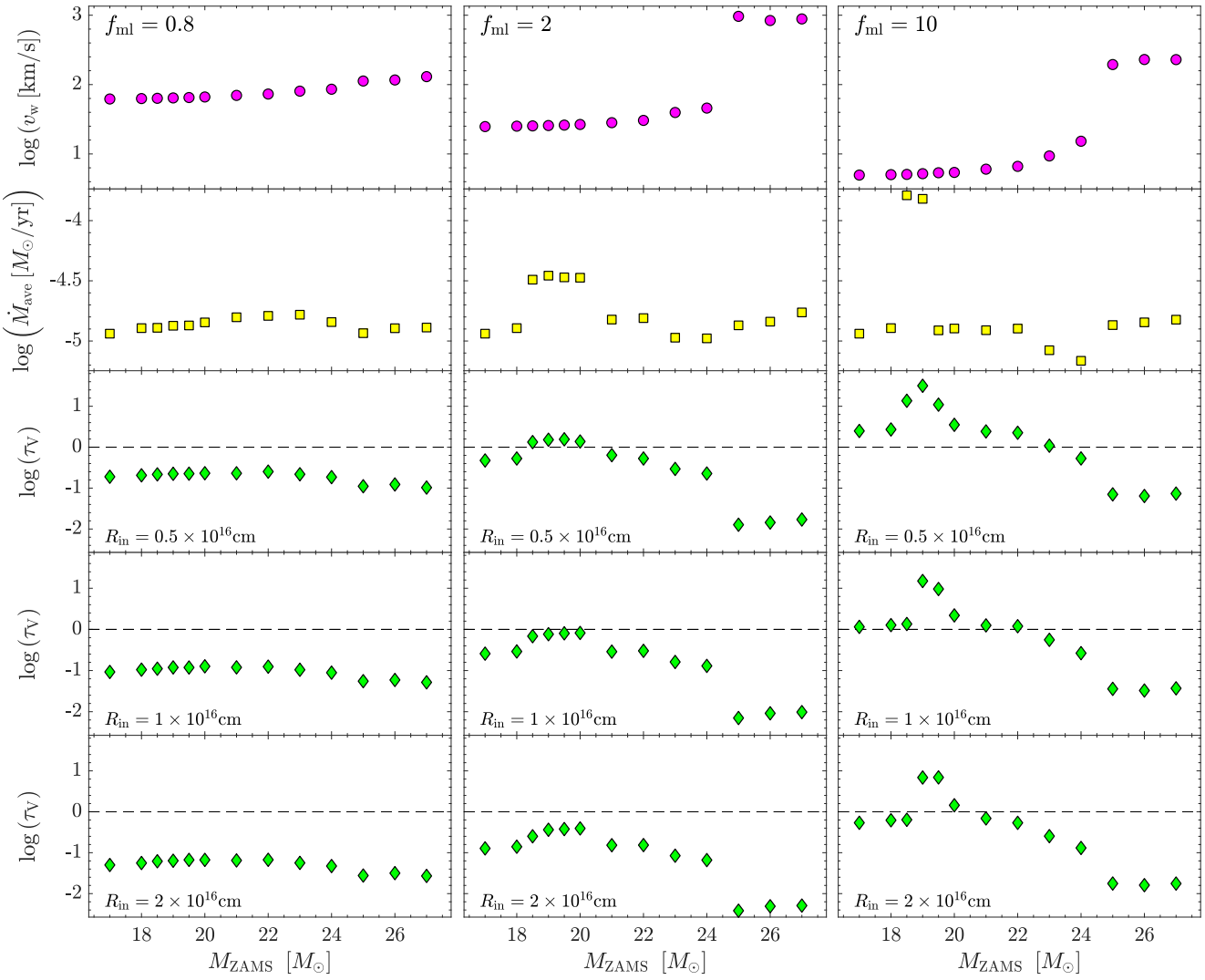

Figure 3. From top row to bottom and in logarithmic scales: The wind velocity according to equation (3), the average mass-loss rate in the last 100 yr before core-collapse, and the optical depth of the dust as given by equation (4) with opacity of $\kappa_{\rm V} = 100\ {\rm cm^2\ g^{-1}}$ and for three values of the inner radius, $R_{\rm in} = 0.5,\ 1,\ 2 \times 10^{16}$ cm; the dashed black line marks: $\tau_{\rm V} = 1$. We calculate each quantity for the three instability strip mass-loss scaling factors $f_{\rm ml} = 0.8$ (left column), $f_{\rm ml} = 2$ (middle column), and $f_{\rm ml} = 10$ (right column).

explosion and its radiation, as well as the collision of the fastest ejecta with the dust). We also take a density of $\rho(r) = \dot{M}/4\pi v_{\rm w} r^2$, where $\dot{M}$ is the mass-loss rate and $v_{\rm w}$ is the wind velocity. We also take the opacity in the V band to be $\kappa_{\rm V} \approx 100\ {\rm cm^2\ g^{-1}}$ (e.g. Kochanek et al. 2012), and derive

$$\tau_{\rm V} = \int_{R_{\rm in}}^{R_{\rm out}} \kappa_{\rm V} \rho\ {\rm d}r \simeq 5 \left(\frac{\dot{M}}{10^{-4} M_\odot\ {\rm yr^{-1}}}\right) \left(\frac{R_{\rm in}}{10^{16}\ {\rm cm}}\right)^{-1} \times \left(\frac{\kappa_{\rm V}}{100\ {\rm cm^2\ g^{-1}}}\right) \left(\frac{v_{\rm w}}{10\ {\rm km\ s^{-1}}}\right)^{-1}, \quad (2)$$

where in the second equality we assume constant mass-loss rate and wind velocity and that $R_{\rm out} \gg R_{\rm in}$.

To derive a more accurate expression, we take the mass-loss rate as function of time from our numerical results. The density, $\rho(r)$, at radius r corresponds to a mass-loss, $\dot{M}(t)$, at time $t = t_{\rm cc} - r/v_{\rm w}$, where $t_{\rm cc}$ is the time of core-collapse (explosion). We take $v_{\rm w}$ constant with time according to the following prescription. We simply assume that when the mass-loss rate in the strip is higher, the wind velocity is lower even after the star leaves the instability strip. For the default mass-loss rate, $f_{\rm ml} = 0.8$, we take the wind velocity to be the escape velocity from the star at core-collapse, $v_{\rm esc,cc}$. The wind velocity is then

$$v_{\rm w} = v_{\rm esc,cc} \left(\frac{f_{\rm ml}}{0.8}\right)^{-1}. \quad (3)$$

Taking $r = v_{\rm w}(t_{\rm cc} - t)$ the expression for the optical depth is

$$\tau_{\rm V} = \int_{t_{\rm out}}^{t_{\rm in}} \frac{\kappa_{\rm V} \dot{M}(t)}{4\pi v_{\rm w}^2 (t_{\rm cc} - t)^2}\ {\rm d}t. \quad (4)$$

We present the wind velocity according to equation (3) for the different models in the top row of Fig. 3. In the second row we present the average mass-loss rate in the last 100 yr before explosion, and in the three bottom rows we present the optical depth according

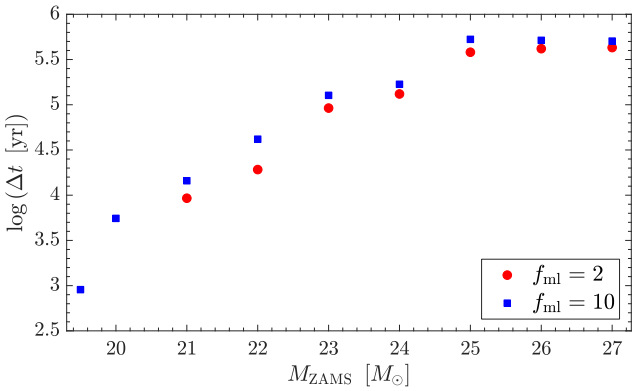

Figure 4. The time of explosion after exiting the instability strip as a function of ZAMS mass.

to equation (4) for $\kappa_{\rm V} = 100$ cm^2 g^{-1}, and for three different values of the inner radius $R_{\rm in} = 0.5, 1, 2 \times 10^{16}$ cm. The differences in the optical depth between the three values of the inner radius are very small, and in what follows we will refer to the numbers for $R_{\rm in} = 10^{16}$ cm. We discuss the implications of the optical depth in Section 4.

Another relevant quantity is the time after the model exists the instability strip and until explosion, which we present in Fig. 4.

Although Meynet et al. (2015) do not consider the RSG problem, it is beneficiary to compare some of our results with theirs. Meynet et al. (2015) enhance the mass-loss rate by a factor of 10 or 25 when the star is an RSG, which they take to be when the effective temperature is $\log(T_{\rm eff}/{\rm K}) < 3.7$. Namely, they do not consider an instability strip, but rather they enhance the mass-loss rate whenever the star has a low effective temperature. They chose these factors somewhat arbitrarily. Another difference is that we use an initial metalicity of $Z = 0.02$ while they take $Z = 0.014$.

In evolution without rotation, the 20 $M_\odot$ stellar models of Meynet et al. (2015) do not have an effective temperature larger than 10^4 K at explosion. We also find that our 20 $M_\odot$ do not reach high temperatures at explosion. Their non-rotating model of 25 $M_\odot$ reaches a temperature of $\log(T_{\rm eff}/{\rm K}) \simeq 4.2$ at the end of the evolution, and with a hydrogen mass of $\lesssim 0.1\,M_\odot$. Our 25 $M_\odot$ model ends with an effective temperature of $\log(T_{\rm eff}/{\rm K}) \simeq 4.2$ and with no hydrogen. Generally, for the more massive stars, $M \gtrsim 25\,M_\odot$, we obtain different results from those of Meynet et al. (2015). They note that their prescription forms no WC stars (WC are WR stars with strong carbon and oxygen emission lines). We, on the other hand, account for WR stars, and possibly for WC stars. Our results are compatible with the suggestion of Shenar et al. (2019) that traditional evolution codes might underestimate mass-loss rates during the RSG phase. Shenar et al. (2019) based their suggestion on their claim that, at least in the Small Magellanic Cloud, the binary evolution channel does not dominate the formation of WR stars.

Overall, our results and those of Meynet et al. (2015) have some similarities, although they are not identical. This is expected because the enhanced mass-loss rate prescription is very different. In any case, the results do not contradict each other. The most important similarity is that both studies conclude that with an enhanced mass-loss rate a significant fraction of massive stars explode as CCSNe while they are hotter than RSGs. This implies that they might not be SNe II and not even SNe IIb.

4 IMPLICATIONS TO THE RSG PROBLEM

In our search for the mass-loss rate that would be necessary to explain the RSG problem for single stars, we increased the mass-loss rate in the extension of the instability strip. We described the results of stellar evolution simulations in Section 3. This introduction of high mass-loss rate in the extension of the instability strip splits the stars that enter the strip from right to left to four groups. (1) Stars that explode while still suffering a very high mass-loss rate and are likely to be IR-bright but visibly faint. These stars fulfil our request that the enhanced mass-loss rate that we introduce forms a CSM that obscures the exploding stars. (2) Stars that leave the strip and explode as SNe II. (3) Stars that leave the strip and explode with hydrogen mass of $0.01\,M_\odot \lesssim M_{\rm H,cc} \lesssim 0.5$–$1\,M_\odot$ and form SNe IIb. (4) Stars that lose all their hydrogen and explode as SNe Ib. We infer the mass range of each group from Figs 2 and 3.

Because of the large uncertainties in mass-loss rates, boundaries of the extension of the instability strip, and a possible influence by weak binary interaction (our scheme does not treat strong binary interaction), we take the boundaries between the groups as whole solar mass, beside one case. We basically give the boundaries between the above groups for the minimum mass-loss rate enhancement that we found to be necessary to account for the RSG problem. Gordon, Humphreys & Jones (2016) argue that 30 per cent to 40 per cent of the yellow supergiants that they study in the galaxies M31 and M33 are likely in a post-RSG phase. The stars that leave the instability strip in our simulations (groups 2–4 above) might account in part for these yellow supergiants.

4.1 Dust enshrouded IR bright CCSNe

From Fig. 3 we see that for $f_{\rm ml} = 10$ in our mass-loss scheme this group comprises stars with initial masses of $M_{\rm S,IR} \approx 18.5$–$20\,M_\odot$. We emphasize that the size of the instability strip in these high luminosities is uncertain, and the range might be somewhat larger. As well, our scheme refers only to single stars and those that suffer a weak binary interaction. Stars with a strong binary interaction require different calculations. In any case, this range of stellar mass ($M_{\rm S,IR} \approx 18.5$–$20\,M_\odot$) is large enough for us to claim that the values of $f_{\rm ml} = 10$ (a factor of 12.5 mass-loss rate enhancement) is about the minimum value that is required for the mass-loss rate enhancement to possibly explain the RSG problem (or part of it).

We assume here and below that about half of the stars suffer only weak or no binary interaction. For an initial mass function (IMF) of $dN \propto M^{-2.35}\,dM$, we find this group to account for $F_{\rm S,IR} \approx 2$ per cent of all CCSNe. With weak binary interactions that enhance mass-loss and somewhat wider instability strip, this group might be $\approx$ 5 per cent of all CCSNe. By a weak binary interaction, we refer to a weak to moderate spin-up by a companion or a weak tidal interaction. Our scheme does not include strong binary interactions where a companion determines the mass-loss rate, e.g. like a massive companion that enters a common envelope.

In discussing an explosion within a dust shell, we follow Kochanek et al. (2012) in treating obscuring by dust. They discuss several important processes, such as the presence of one type of dust, silicate (for massive stars that we study here) or graphitic, and the emission by the dust shell. Since the dust shell is unresolved, its emission adds to the luminosity mainly in the IR. The optical depth in the visible of wind with constant velocity $v_{\rm w}$ and a constant mass-loss rate of $\dot{M}$ is given by equation (2). In the lower row of Fig. 3 we present the optical depth in the V band for a dusty wind that takes into account the mass-loss rate variation in our stellar evolution

simulations (equation 4 from an inner radius $R_{\rm in} = 10^{16}$ cm), but takes a constant wind velocity (equation 3).

Since the shell is not resolved, not all the photons in the visible that are scattered by dust are lost from our beam, and the decrease in the visible light is about a factor of few $\times$ 10 for $\tau_V = 5$, or more than three magnitudes in the visible (Kochanek et al. 2012).

Shortly after the explosion the SN ejecta collides with the dense wind, the CSM. The interaction of the ejecta with the CSM converts kinetic energy to radiation. We scale the efficiency of this process to be $\epsilon_i = 0.1$ and the shock velocity into the CSM to be $v_{\rm s} = 4000$ km s^{-1} (e.g. Fox et al. 2013, 2015)

$$L_i = \epsilon_i \dot{M} \frac{v_{\rm s}^3}{2v_{\rm w}} = 5.3 \times 10^6 \left(\frac{\dot{M}}{10^{-4}\,{\rm M}_\odot\ {\rm yr}^{-1}} \right) \times \left(\frac{v_{\rm s}}{4000\ {\rm km\ s}^{-1}} \right)^3 \left(\frac{v_{\rm w}}{10\ {\rm km\ s}^{-1}} \right)^{-1} \left(\frac{\epsilon_i}{0.1} \right) {\rm L}_\odot. \quad (5)$$

This corresponds to a bolometric magnitude of about -12, fainter by several magnitudes relative to typical CCSNe. In addition, the dust that still resides at large distances will make the SN redder, and so the visual magnitude will be lower even relative to typical CCSNe. Such events might be classified at first place as intermediate luminosity optical transients (ILOTs), rather than CCSNe. But they are fainter in the visible and therefore will be detected in much lower numbers than CCSNe that are not enshrouded by a dense dusty wind.

We conclude that the dusty wind reduces the luminosity in the visible by several magnitudes. Present observations can still detect such type II CCSNe, but at much smaller numbers than their occurrence rate. As we write above, these are only for stars in the initial mass range of $M_{\rm S,IR} \approx 18.5-20\,{\rm M}_\odot$.

4.2 Type II CCSNe

This group is of stars that have hydrogen mass at core-collapse of $M_{\rm H,cc} \gtrsim 1\,{\rm M}_\odot$, and that are not enshrouded by optically thick dust. From Fig. 2 we find the upper mass of this group and from Fig. 3 its lower mass. These give for the mass range of this group $M_{\rm S,II} \simeq 20-21\,{\rm M}_\odot$. This mass range amounts to ≈ 2 per cent of all CCSNe, or $F_{\rm S,II} \approx 1$ per cent of all CCSNe if we take those that do not suffer strong binary interaction.

4.3 Type IIb CCSNe

SNe IIb are CCSNe that in the first several days have strong hydrogen lines, but later these lines substantially weaken and even disappear. This results from low hydrogen mass at explosion, about $M_{\rm H,cc} \simeq 0.03-0.5\,{\rm M}_\odot$ (e.g. Meynet et al. 2015; Yoon, Dessart & Clocchiatti 2017), or even up to $M_{\rm H,env} \leq 1\,{\rm M}_\odot$ (e.g. Sravan, Marchant & Kalogera 2018). SNe IIb make $f_{\rm IIb,H} \simeq 10$–12 per cent of all CCSNe in high metallicity stellar populations (e.g. Sravan et al. 2018). From Fig. 2 we find that the relevant mass range for SNe IIb progenitors in our $f_{\rm ml} = 10$ case is $M_{\rm S,IIb} \simeq 21-24\,{\rm M}_\odot$. Meynet et al. (2015) also find that with their scheme of RSG enhanced mass-loss rate many stars end with low hydrogen mass. For an IMF of ${\rm d}N \propto M^{-2.35}{\rm d}M$ this amounts to $\simeq$0.045 of all CCSNe. However, if about half of these stars suffer strong binary interaction that our scheme does not consider, the single-star and weak binary interaction channels that we study here for SNe IIb correspond to $F_{\rm S,IIb} \approx 2$ per cent of all CCSNe. We note that Naiman et al. (2019) crudely suggest that the single-star channel for SNe IIb accounts for $\approx$ 2–4 per cent all CCSNe (about 20–40 per cent of all SNe IIb).

4.4 Type Ib CCSNe

In the mass range we calculate here this group comes from stars with an initial mass of $M_{\rm S,Ib} \gtrsim 24-25$, as we see from Fig. 2. Meynet et al. (2015) simulated enhanced mass-loss rate from stars up to $M_{\rm ZAMS} = 25\,{\rm M}_\odot$ and find that all of them maintain hydrogen. We find this limit at $M_{\rm ZAMS} = 24\,{\rm M}_\odot$. Consider that we do not use the same mass-loss rate enhancement scheme as they do, this is not a large difference. This range amounts to $\simeq 20$ per cent of all CCSNe if we take the upper mass limit to be $M_{\rm ZAMS} = 100\,{\rm M}_\odot$. If we consider that about half suffer strong binary interaction (e.g. Sana et al. 2012), the single star evolution (including weak binary interactions) that we study here amounts to $F_{\rm S,Ib} \approx 10$ per cent of all CCSNe. Some of them might lose also all their helium and lead to SNe Ic. Our finding that most, $\simeq 2/3$, of the stars with $M_{\rm S,Ib} \gtrsim 18$ form SNe Ib and possibly SNe Ic, is compatible with the finding of Smartt (2015). The claim of Stritzinger et al. (2020) that the progenitor of the SN Ib LSQ13abf had an initial mass of $\gtrsim 25\,{\rm M}_\odot$ (or $\gtrsim 20$–$25\,{\rm M}_\odot$ in an alternative model) supports our claim.

This group of stars adds to the role of the mass-loss rate enhancement in accounting for the RSG problem. Namely, the research question of this study, which is about the enhanced mass-loss rate that is necessary to explain the RSG problem, refers both to obscured CCSNe and to transforming some RSG stars to progenitors of SNe Ibc (Section 1).

The finding above has implications to the rate of formation of WR stars in the single-star channel. Many WR stars are observed to be single, but traditional stellar evolution calculations are short in accounting for these WR stars as well as other properties (e.g. Shenar et al. 2020). For that, some (e.g. Schootemeijer & Langer 2018) claim that the companion in many of these systems is a low-mass star that observations did not reveal yet. However, other studies (e.g. Shenar et al. 2016) suggest that, at least in the Small Magellanic Cloud, the binary evolution channel does not dominate WR formation. Shenar et al. (2019) study WR stars and their formation in the binary and single-stellar channels, and suggest that it is possible that traditional evolution codes underestimate mass-loss (mainly) during the red supergiant phase (for an earlier similar claim see Vanbeveren et al. 1998a; Vanbeveren, De Loore & Van Rensbergen 1998b. Our assumption of an enhanced mass-loss rate in the upper instability strip, and the results of high fraction of SNe Ibc progenitors, are compatible with the claim of Shenar et al. (2019) of a higher mass-loss rate than what traditional evolution code give.

5 SUMMARY

We are motivated by the theoretical disagreement on the fate of star with ZAMS mass of $M_{\rm ZAMS} \gtrsim 18\,{\rm M}_\odot$ (Section 1). For that, we examined the question of what enhanced mass-loss rate during the RSG would be necessary to explain the RSG problem. We noted that there is no support from observations for such a large enhanced mass-loss rate factor. Therefore, we raised a theoretical question. We found that we need to increase the mass-loss rate by at least a factor of about ten (we used a factor of 12.5 in this study) in the instability strip of the RSG to explain the RSG problem (or part of it).

Using the numerical stellar evolution code MESA we have simulated the evolution of 48 stellar models to the point of core-collapse and explored the effect of an enhanced mass-loss inside the instability strip as the evolved stars cross from right to left at very high luminosities. Based on Yoon & Cantiello (2010) we assumed an

enhanced mass-loss rate as the star crosses the instability strip from right to left at high luminosities (grey area of the instability strip in Fig. 1). Our mass-loss prescription is for single star evolution and possibly weak binary interaction. We do not include strong binary interaction.

We concentrated on two pre-core-collapse stellar properties, the stellar hydrogen mass (Fig. 2), and the optical depth of the dusty wind (Fig. 3). From these properties we divide the stars that enter or cross the upper (extension) instability strip to four groups with very uncertain mass boundaries between them. (1) Stars that explode as SNe II while they are in the strip and therefore are enshrouded by dust (Section 4.1). These have initial mass in the range of $M_{\rm S,IR} \simeq 18.5{-}20\,{\rm M}_\odot$. (2) Stars that leave the instability strip from the left and explode as SNe II. They have $M_{\rm S,II} \simeq 20{-}21\,{\rm M}_\odot$ (Section 4.2). (3) Stars that leave the strip and at core-collapse have a hydrogen mass of $M_{\rm H,cc} \lesssim 0.5{-}1 M_\odot$. They explode as SNe IIb and have $M_{\rm S,\,IIb} \simeq 21{-}24\,{\rm M}_\odot$ (Section 4.3). (4) Stars that leave the strip and explode as SNe Ib and possibly as SNe Ic. These have $M_{\rm S,Ib} \gtrsim 24$ (Section 4.4).

In short, we have found that an enhanced mass-loss rate in the instability strip (Fig. 1) by a factor of about 10 or more, helps solving the RSG problem by causing some CCSN to be obscured by dust (group 1 above) and by causing other stars to explode as SNe Ibc (group 4 above).

Because the mass boundaries of the four groups are highly uncertain, so are the fraction $F_{\rm S}$ of each group is highly uncertain. For the minimum mass-loss rate enhancement that would be necessary to solve the RSG problem, our estimated fractions of CCSNe in each of these four groups are $F_{\rm S,IR} \approx 2$ per cent, $F_{\rm S,II} \approx 1$ per cent, $F_{\rm S,IIb} \approx 2$ per cent, and $F_{\rm S,Ib} \approx 10$ per cent, respectively. In estimating these fractions we used the IMF of $dN \propto M^{-2.35} dM$ with a maximum mass of $100\,{\rm M}_\odot$ and assumed that about half of the stars suffer strong binary interaction that we do not consider here. Therefore, our assumption of enhanced mass-loss while in the instability strip implies that single star evolution brings only a fraction of

$$\eta_{\rm S,II} \equiv \frac{F_{\rm S,II}+F_{\rm S,IIb}}{F_{\rm S,IR}+F_{\rm S,II}+F_{\rm S,IIb}+F_{\rm S,Ib}} \approx 20 \text{ per cent} \qquad (6)$$

of stars with $M_{\rm ZAMS} \gtrsim 18.5\,{\rm M}_\odot$ to end as SNe II or SNe IIb that are not heavily enshrouded by dusty CSM.

Smartt (2015) lists 30 progenitors of SN type II or IIb which all have a ZAMS mass of $M_{\rm ZAMS} \lesssim 18\,{\rm M}_\odot$. From that he argues that the IMF implies that if all these stars explode there should be ≈13 CCSNe of types II and IIb with a progenitor of $M_{\rm ZAMS} \gtrsim 18\,{\rm M}_\odot$. According to our analysis (equation 6) we expect that out of these 13 SNe with progenitor mass $M_{\rm ZAMS} \gtrsim 18\,{\rm M}_\odot$, only ≈2−3 are SNe II or IIb (and binary interaction can reduce this number further by forming more SNe Ibc).[1]

Our main conclusion is that the statistical uncertainties are too large to decide whether many stars with $M_{\rm ZAMS} \gtrsim 18\,{\rm M}_\odot$ do not explode as expected in the neutrino driven explosion mechanism, or whether most of them form SNe Ibc and obscured SNe II that are IR-bright, as expected by the jittering jets explosion mechanism.

[1]At the Symposium 'The Deaths and Afterlives of Stars' (Space Telescope Science Institute, April 22–24, 2019), Smartt updated the observed number of progenitors with $M_{\rm ZAMS} \lesssim 18\,{\rm M}_\odot$ to 35 (https://cloudproject.hosted.panopto.com/Panopto/Pages/Viewer.aspx?id=d6217958-cb9c-4825-8005-aa3700f5dfb0). In this case, 15 progenitors with a mass of $M_{\rm ZAMS} \gtrsim 18\,{\rm M}_\odot$ are expected. By our analysis, only three of them should be type II or IIb CCSNe.

ACKNOWLEDGEMENTS

We thank an anonymous referee for detailed and useful comments. This research was supported by a grant from the Israel Science Foundation. Research of Noam Soker is partially supported by the Charles Wolfson Academic Chair.

REFERENCES

Adams S. M., Kochanek C. S., Gerke J. R., Stanek K. Z., Dai X., 2017, MNRAS, 468, 4968
Beasor E. R., Davies B., Smith N., van Loon J. T., Gehrz R. D., Figer D. F., 2020, MNRAS, 492, 5994
Bethe H. A., Wilson J. R., 1985, ApJ, 295, 14
Blondin J. M., Mezzacappa A., 2007, Nature, 445, 58
Brott I. et al., 2011, A&A, 530, A115
Couch S. M., Ott C. D., 2013, ApJ, 778, L7
Couch S. M., Ott C. D., 2015, ApJ, 799, 5
de Jager C., Nieuwenhuijzen H., van der Hucht K. A., 1988, A&AS, 72, 259
Ertl T., Janka H.-T., Woosley S. E., Sukhbold T., Ugliano M., 2016, ApJ, 818, 124
Ertl T., Woosley S. E., Sukhbold T., Janka H.-T., 2020, ApJ, 890, 51
Farmer R., Fields C. E., Petermann I., Dessart L., Cantiello M., Paxton B., Timmes F. X., 2016, ApJS, 227, 22
Fernández R., 2015, MNRAS, 452, 2071
Fox O. D., Filippenko A. V., Skrutskie M. F., Silverman J. M., Ganeshalingam M., Cenko S. B., Clubb K. I., 2013, AJ, 146, 2
Fox O. D. et al., 2015, MNRAS, 454, 4366
Fryer C. L., 1999, ApJ, 522, 413
Georgy C., 2012, A&A, 538, L8
Georgy C. et al., 2013, A&A, 558, A103
Gerke J. R., Kochanek C. S., Stanek K. Z., 2015, MNRAS, 450, 3289
Gilkis A., Soker N., 2014, MNRAS, 439, 4011
Gilkis A., Soker N., 2015, ApJ, 806, 28
Gilkis A., Soker N., Papish O., 2016, ApJ, 826, 178
Glebbeek E. et al., 2009, A&A, 497, 255
Goldman S. R. et al., 2017, MNRAS, 465, 403
Gordon M. S., Humphreys R. M., Jones T. J., 2016, ApJ, 825, 50
Heger A. et al., 1997, A&A, 327, 224
Henyey L., Vardya M. S., Bodenheimer P., 1965, ApJ, 142, 841
Horiuchi S., Nakamura K., Takiwaki T., Kotake K., Tanaka M., 2014, MNRAS, 445, L99
Iwakami W., Nagakura H., Yamada S., 2014, ApJ, 793, 5
Jencson J. E. et al., 2017, ApJ, 837, 167
Jencson J. E. et al., 2019, ApJ, 886, 40
Jennings Z. G., Williams B. F., Murphy J. W., Dalcanton J. J., Gilbert K. M., Dolphin A. E., Weisz D. R., Fouesneau M., 2014, ApJ, 795, 170
Kashi A., Soker N., 2017, MNRAS, 467, 3299
Kazeroni R., Guilet J., Foglizzo T., 2017, MNRAS, 471, 914
Kochanek C. S., Khan R., Dai X., 2012, ApJ, 759, 20
Kuroda T., Takiwaki T., Kotake K., 2014, Phys. Rev. D, 89, 044011
Kushnir D., 2015, preprint (arXiv:1506.02655)
Langer N., Fricke K. J., Sugimoto D., 1983, A&A, 126, 207
Lovegrove E., Woosley S. E., 2013, ApJ, 769, 109
Maeder A., Meynet G., 2001, A&A, 373, 555
Meynet G. et al., 2015, A&A, 575, A60
Mueller B., Janka H.-T., 2015, MNRAS, 448, 2141
Müller B., Melson T., Heger A., Janka H.-T., 2017, MNRAS, 472, 491
Müller B. et al., 2019, MNRAS, 484, 3307
Nadezhin D. K., 1980, Ap&SS, 69, 115
Naiman B., Sabach E., Gilkis A., Soker N., 2020, MNRAS, 491, 2736
Nugis T., Lamers H. J. G. L. M., 2000, A&A, 360, 227
Papish O., Nordhaus J., Soker N., 2015, MNRAS, 448, 2362
Paxton B., Bildsten L., Dotter A., Herwig F., Lesaffre P., Timmes F., 2011, ApJS, 192, 3
Paxton B. et al., 2013, ApJS, 208, 4
Paxton B. et al., 2015, ApJS, 220, 15

Paxton B. et al., 2018, ApJS, 234, 34
Quataert E., Lecoanet D., Coughlin E. R., 2019, MNRAS, 485, L83
Sana H. et al., 2012, Science, 337, 444
Schootemeijer A., Langer N., 2018, A&A, 611, A75
Shenar T. et al., 2016, A&A, 591, A22
Shenar T. et al., 2019, A&A, 627, A151
Shenar T., Gilkis A., Vink J. S., Sana1 H., Sander A. A. C., 2020, A&A, 634, A79
Smartt S. J., 2015, PASA, 32, e016
Smartt S. J., Eldridge J. J., Crockett R. M., Maund J. R., 2009, MNRAS, 395, 1409
Smith N. et al., 2011, ApJ, 732, 63
Soker N., 2010, MNRAS, 401, 2793
Soker N., 2016, New Astron. Rev., 75, 1
Soker N., 2018, preprint (arXiv:1805.03447)
Soker N., 2019a, Research in Astronomy and Astrophysics, 19, 095
Soker N., 2019b, preprint (arXiv:1907.13312)
Sravan N., Marchant P., Kalogera V., 2019, ApJ, 885, 130
Stritzinger M. D., Taddia F., Holmbo S. et al., 2020, A&A, 634, A21
Sukhbold T., Adams S., 2020, MNRAS, 492, 2578
Sukhbold T., Ertl T., Woosley S. E., Brown J. M., Janka H.-T., 2016, ApJ, 821, 38
Van Dyk S. D. et al., 2018, ApJ, 860, 90
Vanbeveren D., De Donder E., Van Bever J., Van Rensbergen W., De Loore C., 1998a, New Astron., 3, 443
Vanbeveren D., De Loore C., Van Rensbergen W., 1998b, A&AR, 9, 63
Vink J. S., de Koter A., Lamers H. J. G. L. M., 2001, A&A, 369, 574
Walmswell J. J., Eldridge J. J., 2012, MNRAS, 419, 2054
Williams B. F., Peterson S., Murphy J., Gilbert K., Dalcanton J. J., Dolphin A. E., Jennings Z. G., 2014, ApJ, 791, 105
Yoon S.-C., Cantiello M., 2010, ApJ, 717, L62
Yoon S.-C., Dessart L., Clocchiatti A., 2017, ApJ, 840, 10

This paper has been typeset from a TEX/LATEX file prepared by the author.